Bhattacharya, Kunal; Chakraborty, Abhijit

Aggregation of self-propelled particles with sensitivity to local order

Published in:
Physical Review E

DOI:
10.1103/PhysRevE.105.044124

Published: 15/04/2022

Document Version
Publisher's PDF, also known as Version of record

Aggregation of self-propelled particles with sensitivity to local order

Kunal Bhattacharya [1,2] and Abhijit Chakraborty [3,4,*]

[1]*Department of Industrial Engineering and Management, Aalto University School of Science, 00076 Aalto, Finland*
[2]*Department of Computer Science, Aalto University School of Science, 00076 Aalto, Finland*
[3]*Complexity Science Hub Vienna, Josefstaedter Strasse 39, 1080 Vienna, Austria*
[4]*Graduate School of Advanced Integrated Studies in Human Survivability, Kyoto University, 1 Nakaadachi-cho, Yoshida, Sakyo-ku, Kyoto 606-8306, Japan*

(Received 2 May 2021; revised 31 December 2021; accepted 16 March 2022; published 15 April 2022)

We study a system of self-propelled particles (SPPs) in which individual particles are allowed to switch between a fast aligning and a slow nonaligning state depending upon the degree of the alignment in the neighborhood. The switching is modeled using a threshold for the local order parameter. This additional attribute gives rise to a mixed phase, in contrast to the ordered phases found in clean SPP systems. As the threshold is increased from zero, we find the sudden appearance of clusters of nonaligners. Clusters of nonaligners coexist with moving clusters of aligners with continual coalescence and fragmentation. The behavior of the system with respect to the clustering of nonaligners appears to be very different for values of low and high global densities. In the low density regime, for an optimal value of the threshold, the largest cluster of nonaligners grows in size up to a maximum that varies logarithmically with the total number of particles. However, on further increasing the threshold the size decreases. In contrast, for the high density regime, an initial abrupt rise is followed by the appearance of a giant cluster of nonaligners. The latter growth can be characterized as a continuous percolation transition. In addition, we find that the speed differences between aligners and nonaligners is necessary for the segregation of aligners and nonaligners.

DOI: 10.1103/PhysRevE.105.044124

I. INTRODUCTION

Collective motion observed in diverse natural and artificial systems has been the subject of numerous experimental and theoretical investigations. Systems that have been studied include fish schools [1], birds flocks [2], bacterial colonies [3], human crowds [4], as well as, synthetic microswimmer assemblies [5] and robotic swarms [6]. Local interactions in such systems are understood to lead to the emergence of global order or flocking states. This has been demonstrated in self-propelled particle (SPP) models in which particles are attributed the tendency to align their direction of motion with their immediate spatial neighbors in the presence of noise [7]. Recent studies have also focused on the possible effects of environmental and individual-level inhomogeneity on the flocking dynamics [8–10]. For example, disorder is introduced in SPP models in the form of spatially distributed obstacles [8,11], or a finite fraction of the particles is made nonaligners [9,10]. The dynamics in these systems shows the development of phases with complex features like quasi-long-range order [8] and self-sorting [9]. In natural flocks, the latter type of inhomogeneity could result from differences in signaling and receptive behavior or conflict in intentions. In an otherwise homogeneous flock, behavioral shifts at individual levels could imply a certain fraction of flock members spontaneously modifying their nature of motion.

Flocks of living organisms are known to arrange themselves into cohesive and sometimes segregated units while performing activities like foraging and migration [12–14]. This is achieved through consensus decision-making by flock members while performing the activities that, in turn, are a consequence of mechanisms at the level of individuals. Such behavioral transitions between different states have been documented in various species [15–18]. Suitable modifications to simple SPP models have proven to be useful in reproducing the spatiotemporal features of flocks with behavioral shifts. Models have considered additional attributes to SPPs, like adaptive speed [15,19,20], random fields [21], and transition rates [18].

Experiments on fish schooling [22,23] and bacterial suspensions [24] have shown that individual speeds can vary depending on the local order parameter (polarization). A model motivated by these experiments considered SPPs with alignment interactions and a power-law dependence of the speed on the local polarization [25,26]. This showed the nucleation of static clusters and an inverse correlation between the speed and the local density. Notably, for SPP systems without alignment such a speed-density relationship leads to a motility-induced phase separation (MIPS) [27] whereby two phases with distinct densities coexist in the system. This is known to arise from the feedback between the slowing down and crowding of the particles. In general, the variability in the speed both in the absence [28–30] and in the presence [20,31–34] of alignment has been shown to result in novel complex phenomena in models and experiments.

*Corresponding author: chakraborty.abhijit.7y@kyoto-u.ac.jp

In this paper we study an SPP model in which particles can switch between a fast aligning state and a slow nonaligning state depending on the local orientational order parameter. An aligner becomes a nonaligner once the local polarization falls below a threshold $\phi_{\rm th}$, and conversely, a nonaligner becomes an aligner if the local polarization rises above $\phi_{\rm th}$. Using the model, we illustrate a mechanism in which processing of local information allows an SPP system to simultaneously organize into polarized moving clusters as well as aggregations. The collisions between clusters play a crucial role in such phase separation, as we explain later. With our numerical analyses we primarily focus on characterizing the clustering behavior.

In the absence of a threshold, or, equivalently, with $\phi_{\rm th} \to 0$, the model expectedly shows an order to disorder transition with the increase in noise [7,35]. We find that the introduction of a finite threshold has a complex interplay with this transition. In the steady state, the model with $\phi_{\rm th} > 0$ permits clusters of aligners to coexist with those of nonaligners. The dynamics are found to crucially depend on the level of the noise, the value of $\phi_{\rm th}$, and the overall density. At low noise, the aggregation behavior of nonaligners can be broadly categorized into two different regimes. For low enough densities, an optimal value of $\phi_{\rm th}$ is found to limit the growth of the largest cluster of nonaligners; at higher densities the latter is able to grow macroscopically large when $\phi_{\rm th}$ is increased.

Recent studies have considered SPP models relevant to the understanding of epidemic and information spreading in populations of motile agents [36,37]. The particles could either irreversibly or reversibly switch between motile and nonmotile states and collectively exhibited fractal aggregation and MIPS. These models considered switching rules based on logic gates involving the states of colliding particles. In contrast, the particles in our model change their states depending upon the orientations of their neighbors.

The outline of the paper is as follows. We explain the details of the model in Sec. II. In Sec. III we discuss the results of our numerical investigation, and in Sec. IV we conclude with a summary and final observations.

II. THE MODEL

We consider N self-propelled particles moving on a two-dimensional square area of linear size L under periodic boundary conditions. The global density of the system is given by $\rho = N/L^2$. At discrete times t, the state of the ith particle is given by its position $\mathbf{r}_i^t$, angle of the direction of motion θ_i^t, and s_i^t, which denotes an aligner ($s_i^t = 1$) or nonaligner ($s_i^t = 0$). The variables are updated in the following way. First, the set of neighbors $\mathcal{N}_i$ of the ith particle is enumerated, which comprises of all the particles that are within a distance of r_0 from i. Then the local order parameter ϕ_i, which is the average normalized velocity within the neighborhood, is calculated as

$$\phi_i^t = \frac{1}{1+k_i}\left|\mathbf{n}_i^t + \sum_{j\in\mathcal{N}_i}\mathbf{n}_j^t\right|. \tag{1}$$

Here, $\mathbf{n}_i^t = (\cos\theta_i^t, \sin\theta_i^t)$ is a unit vector pointing in the direction of motion of i, and k_i is the number of neighbors of i. Whether the particle i would have the tendency to align its direction of motion with its neighbors is decided depending on ϕ_i^t:

$$s_i^{t+1} = \begin{cases} 0 & \text{if } \phi_i^t \leqslant \phi_{\rm th}, \\ 1 & \text{if } \phi_i^t > \phi_{\rm th}, \end{cases} \tag{2}$$

where $\phi_{\rm th}$ is a parameter in the model. Last, the angle of heading and the position are updated according to

$$\theta_i^{t+1} = \arg\left[\mathbf{n}_i^t + s_i^{t+1}\sum_{j\in\mathcal{N}_i}\mathbf{n}_j^t + \alpha\sum_{j\in\mathcal{N}_i} f_{ij}^t\hat{\mathbf{r}}_{ij}^t\right] + \eta\xi_i^t, \tag{3}$$

$$\mathbf{r}_i^{t+1} = \mathbf{r}_i^t + v\big(s_i^{t+1}\big)\mathbf{n}_i^{t+1}, \tag{4}$$

where $v(s_i^{t+1})$ is the magnitude of the velocity depending on whether the particle i is an aligner or a nonaligner, f_{ij}^t is the interaction force between i and its neighbor j, $\hat{\mathbf{r}}_{ij}^t$ is a unit vector from i towards j, α is the strength of the interaction, $\xi_i^t \in [-\pi, \pi]$ is a delta-correlated angular noise, and η is the amplitude of the noise. For an aligner, the dynamics represented in Eqs. (3) and (4) is similar to the Vicsek model [7] with an additional short-range interaction between particles [35,38,39]. For a nonaligner the second term inside the brackets in Eq. (3) is absent.

The force f_{ij} depends on the distance of separation $r_{ij} = |\mathbf{r}_i - \mathbf{r}_j|$ and comprises finite repulsive and attractive terms:

$$f_{ij} = \begin{cases} -f_r\frac{r_e - r_{ij}}{r_e} & \text{if } r_{ij} < r_e, \\ \frac{r_{ij}-r_e}{r_a-r_e} & \text{if } r_e < r_{ij} < r_a, \\ \frac{r_0-r_{ij}}{r_0-r_a} & \text{if } r_a < r_{ij} < r_0, \end{cases} \tag{5}$$

where r_e is the equilibrium distance, r_a is the distance at which attraction is maximum, and f_r is the relative magnitude of the repulsive force when $r_{ij} = 0$. The two-body interaction helps to maintain a finite packing density of particles similar to some of the systems [31,34] in which MIPS-like phenomena are evidenced.

In the simulations, we fix the following values for the parameters: $r_0 = 1$, $r_a = 0.625$, $r_e = 0.25$, $f_r = 1000$, and $\alpha = 0.1$. For the nonaligners, we will consider only the repulsive interaction to be present. Most of the results, unless otherwise specified, are obtained with aligner speed $v_1 = 0.05$, nonaligner speed $v_0 = 0.005$, and noise $\eta = 0.20$. Note that in Eq. (1), $k_i = 0$ implies $\phi_i \equiv 1$, and hence, a nonaligner can switch to the aligning state if it becomes isolated. To ensure that switching arises only as a consequence of interactions in the neighborhood, we prevent isolated nonaligners from switching states. However, for the parameter ranges that we investigate, this additional rule does not influence the macroscopic behavior of the system.

III. RESULTS

At low noise and in the absence of a threshold ($\phi_{\rm th} = 0$) the system is in a globally ordered state with a single macroscopically large cluster of aligners ($s_i = 1$). With the introduction of the switching behavior ($\phi_{\rm th} > 0$), the state of the particles become sensitive to fluctuations occurring locally, and as a result the nonaligners ($s_i = 0$) start appearing in the system and are eventually separated from aligners due to the difference in speeds. In the steady state, we find the system to be

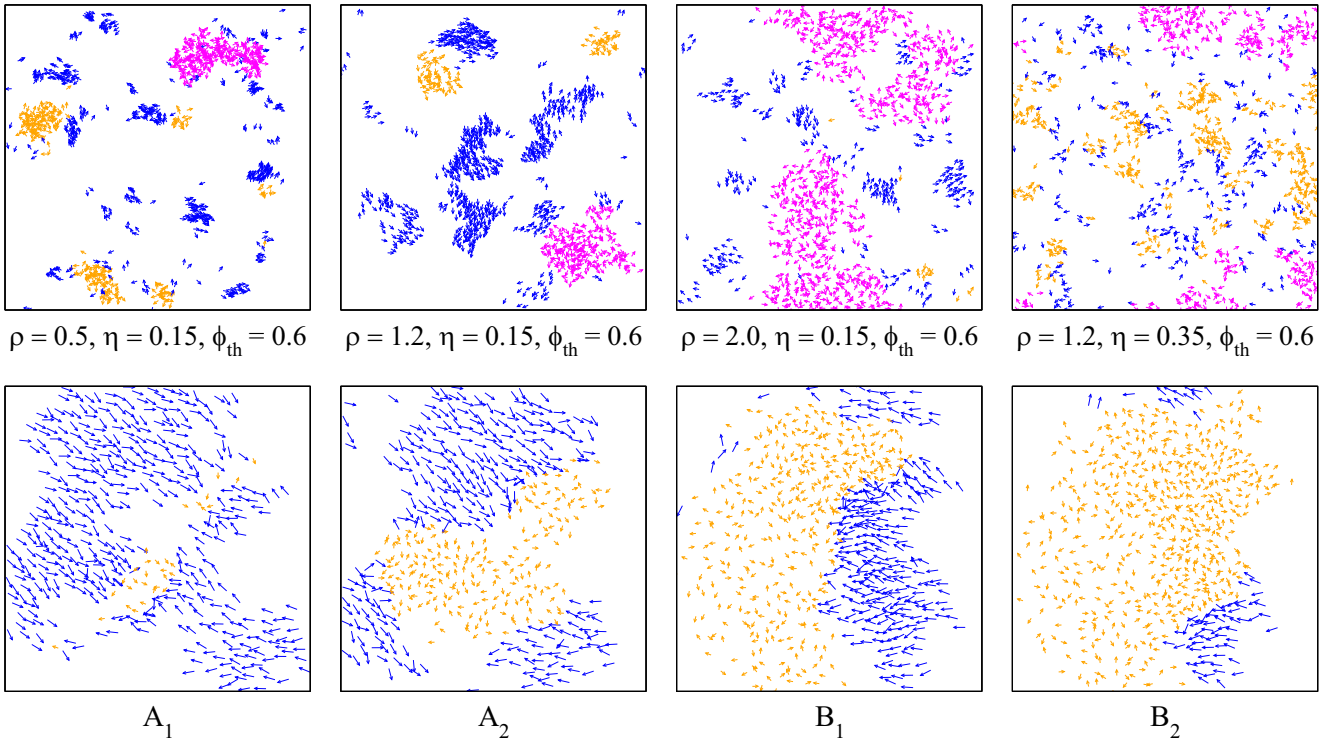

FIG. 1. Snapshots of the dynamics are shown. The top row corresponds to different parameter sets. The first three (from the left) snapshots illustrate the effect of increasing the density ρ, such that, in the third we find an emerging giant cluster of nonaligners. The aligners are denoted in blue (dark gray), and the nonaligners are in orange (light gray). The direction of a vector points to the instantaneous direction of motion. Particles belonging to the largest cluster of nonaligners are marked in magenta (medium gray). In the fourth snapshot, the effect of increasing the noise η is shown. In the bottom row, snapshots A_1 and A_2 illustrate the mechanism of the emergence of cluster of nonaligners from the collision of two moving clusters of aligners. Snapshots B_1 and B_2 show the growth of a cluster of nonaligners when a moving cluster of aligners gets impacted. For both pairs (A_1, A_2 and B_1, B_2), the separation in time is 50 steps, which is equivalent to 2.5 units measured in the timescale r_0/v_1. The number of particles in all the snapshots is $N = 1024$. For the bottom row, $\rho = 1.2$, $\eta = 0.15$, and $\phi_{\text{th}} = 0.6$. Movies corresponding to the first three snapshots are provided in the Supplemental Material [40].

phase separated into moving clusters of aligners and diffusing clusters of nonaligners. If we observe the system in the very dilute limit, $\rho < 0.1$, and with $\phi_{\text{th}} = 0$, we observe a phase with very small sized clusters of aligners due to the short-range two-body force [39]. This is different from the gaseous phase predicted for the original Vicsek model [41,42]. This also implies that for higher densities and for finite ϕ_{th} the large clusters of aligners have a higher chance to coexist alongside clusters of nonaligners.

Our definition of a cluster is based on connecting neighboring particles that are in similar states ($r_{ij} < r_0$ and $s_i = s_j$). In Fig. 1 (top row) we show snapshots of steady state configurations resulting from different parameter values. Large fluctuations in ϕ_i^t primarily occur as a result of collisions between clusters. Clusters of nonaligners form and grow when moving clusters of aligners collide among themselves or with clusters of nonaligners. This process is illustrated in the bottom row of Fig. 1. Similarly, when a moving cluster of aligners grazes a cluster of nonaligners, particles at the boundary of the latter switch their states in a short time span to become aligners. Switching of particles at the boundary of a cluster of nonaligners also happens as random events. To describe the generic properties of the system we measure the sizes of the largest clusters of aligners and nonaligners as functions of overall density and speed of the particles.

A. Low density regime: Dependence on threshold and noise

In Fig. 2 we show the behavior of system at a density $\rho = 0.5$. The aggregation of nonaligners is possible only when the corresponding clean SPP system is in the ordered phase. A small, but finite, η ensures the presence of clusters of aligners moving in different directions which can collide and allow clusters of nonaligners to nucleate. The latter cannot happen when η is large and the system is in a gas-like phase in which large clusters of aligners are absent. This is evidenced in Fig. 2(a), where we show the dependence of the size of the largest cluster of nonaligners M_0 on η and ϕ_{th}. The plot also shows that M_0 attains its maximum around $\phi_{\text{th}} = 0.6$ and $\eta = 0.2$.

For the individual particles in a cluster of aligners ϕ_i^t is high in the ordered phase. However, during the collisions ϕ_i^t for particles at the border of the colliding peripheries decreases momentarily. If the drop in ϕ_i^t is less than ϕ_{th}, then aligners switch and become nonaligners. Therefore, an increase of ϕ_{th} leads to an increase of switching events. For aligners we measure the rate of switching as the number of switches to nonaligning states per unit time per aligner. Similarly, we measure the switching rate for nonaligners. As Fig. 2(b) shows, this rate for aligners increases with ϕ_{th} and decreases for nonaligners. Initially, at low ϕ_{th} the rate is much higher for nonaligners, implying nonaligners do not persist and

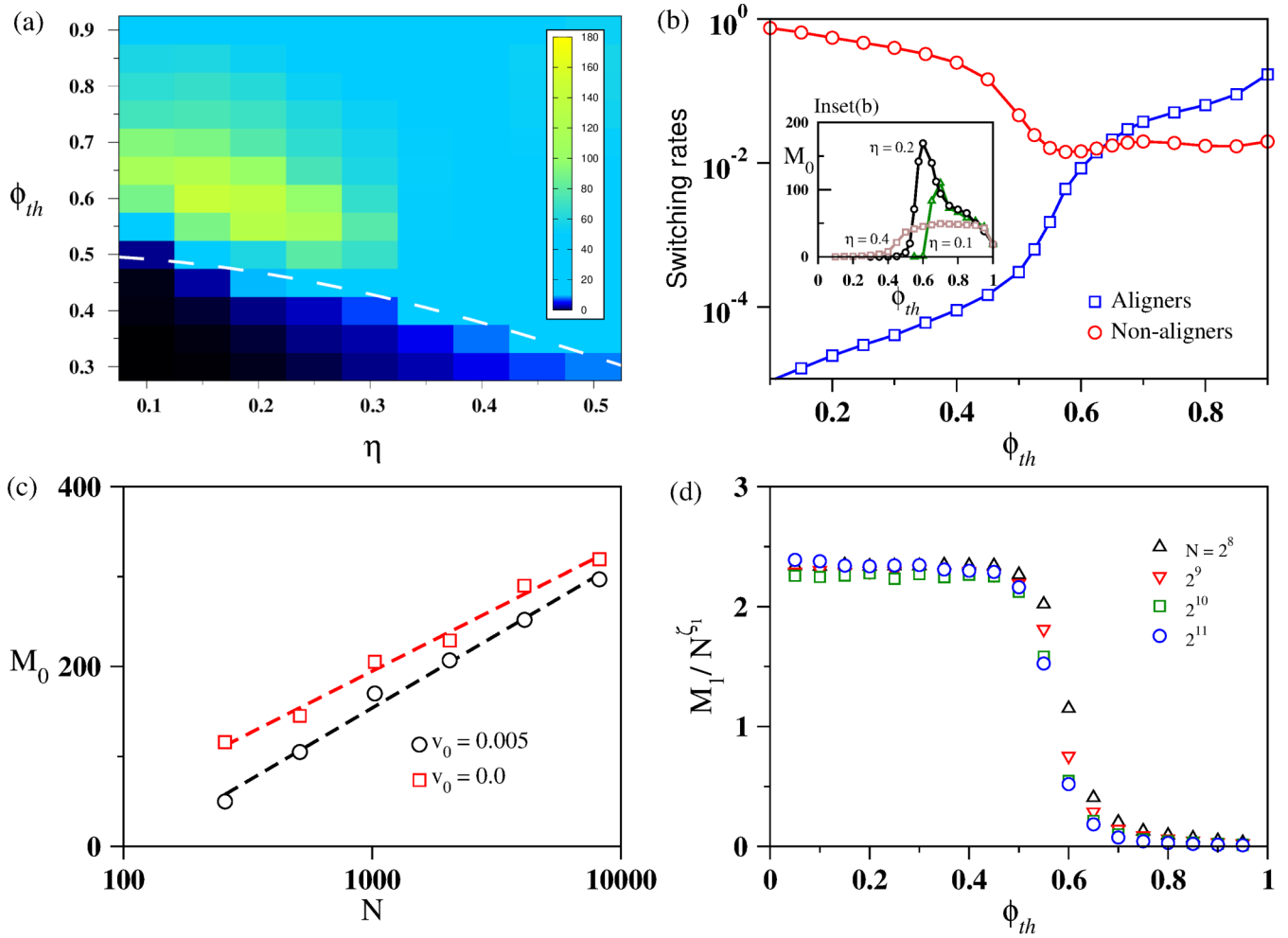

FIG. 2. Sizes of the largest clusters of nonaligners (M_0) and aligners (M_1) are characterized at density $\rho = 0.5$. (a) The dependence of M_0 on noise amplitude η and threshold ϕ_{th} is shown as a heat map for $N = 2^{10}$. The dashed line represents the equation $\phi_{\text{th}} = \phi^*(\eta)$, where $\phi^*(\eta)$ is given by Eq. (6). (b) The rate of switching per unit time per particle is plotted against ϕ_{th} for $N = 2^{10}$ at $\eta = 0.2$. Here, the aligners are switching to nonaligners, and vice versa. The inset shows the variation of M_0 with ϕ_{th} for three noise amplitudes. The maximum of M_0 for $\eta = 0.2$ occurs at $\phi_{\text{th}} \sim 0.6$, which corresponds to the crossing of the switching rates. (c) The dependence of M_0 on N is shown, where M_0 is measured at $\phi_{\text{th}} = 0.6$ and $\eta = 0.2$. In addition to the nonaligner speed $v_0 = 0.005$, the dependence is also shown for $v_0 = 0.0$. The dashed lines represent ordinary least squares fits having the form $M_0 = c_0 + c_1 \log N$. For $v_0 = 0.005$, $c_0 = -225(24)$, and $c_1 = 60(3)$; for $v_0 = 0.0$, $c_0 = -333(22)$, and $c_1 = 70(3)$. (d) The dependence of the size of the largest cluster of aligners M_1 on ϕ_{th} at $\eta = 0.2$. The different symbols correspond to different values of N, as indicated in the legend. Data collapse is obtained by scaling M_1 by the corresponding N^{ζ_1} with $\zeta_1 = 0.78$.

proliferate and, when formed, almost instantly switch back to being aligners. But at higher values of ϕ_{th} the switching rate for aligners overtakes that for nonaligners. This aspect is also reflected when M_0 versus ϕ_{th} is examined in detail. As shown in the inset in Fig. 2(b), for different η's, M_0 has a sharp rise at ϕ_{th} and then reaches a maximum. For $\eta = 0.2$ the maximum occurs at around $\phi_{\text{th}} = 0.6$ and coincides with the point where the rates cross each other. The sharp rise in M_0 is also found to be noise dependent. Note that the switching rate for the nonaligners becomes relatively a constant when ϕ_{th} is large. This is because inside the bulk of a cluster the average separation is r_e, which also implies the number of neighbors for a particle is $k \sim r_0^2/(r_e/2)^2$. With k randomly oriented neighbors inside a cluster of nonaligners the local order parameter takes the typical value of $\phi \sim 1/\sqrt{k} \sim r_e/(2r_0)$ in the steady state [43].

An approximation of the value of the ϕ_{th} for which M_0 sharply rises can be found in the following way. We consider a nonaligner on a colliding boundary as illustrated in Fig. 1 (bottom row). We assume that, on average, half of the neighbors are nonaligners and the rest are aligners. Therefore, the value of the local order parameter can be approximated as

$$\phi^*(\eta) = \frac{1}{2}\frac{\sin \eta\pi}{\eta\pi}, \tag{6}$$

where the expression to the right is half the polar order in an SPP system at low noise and at sufficiently high densities [44,45]. The equation $\phi_{\text{th}} = \phi^*(\eta)$ is shown as a dashed line in Fig. 2(a).

In Fig. 2(c) we find that the maximum values of M_0 increase as $\log N$. In the same plot we show the case with $v_0 = 0$, in which the nonaligners can rotate but not move. The

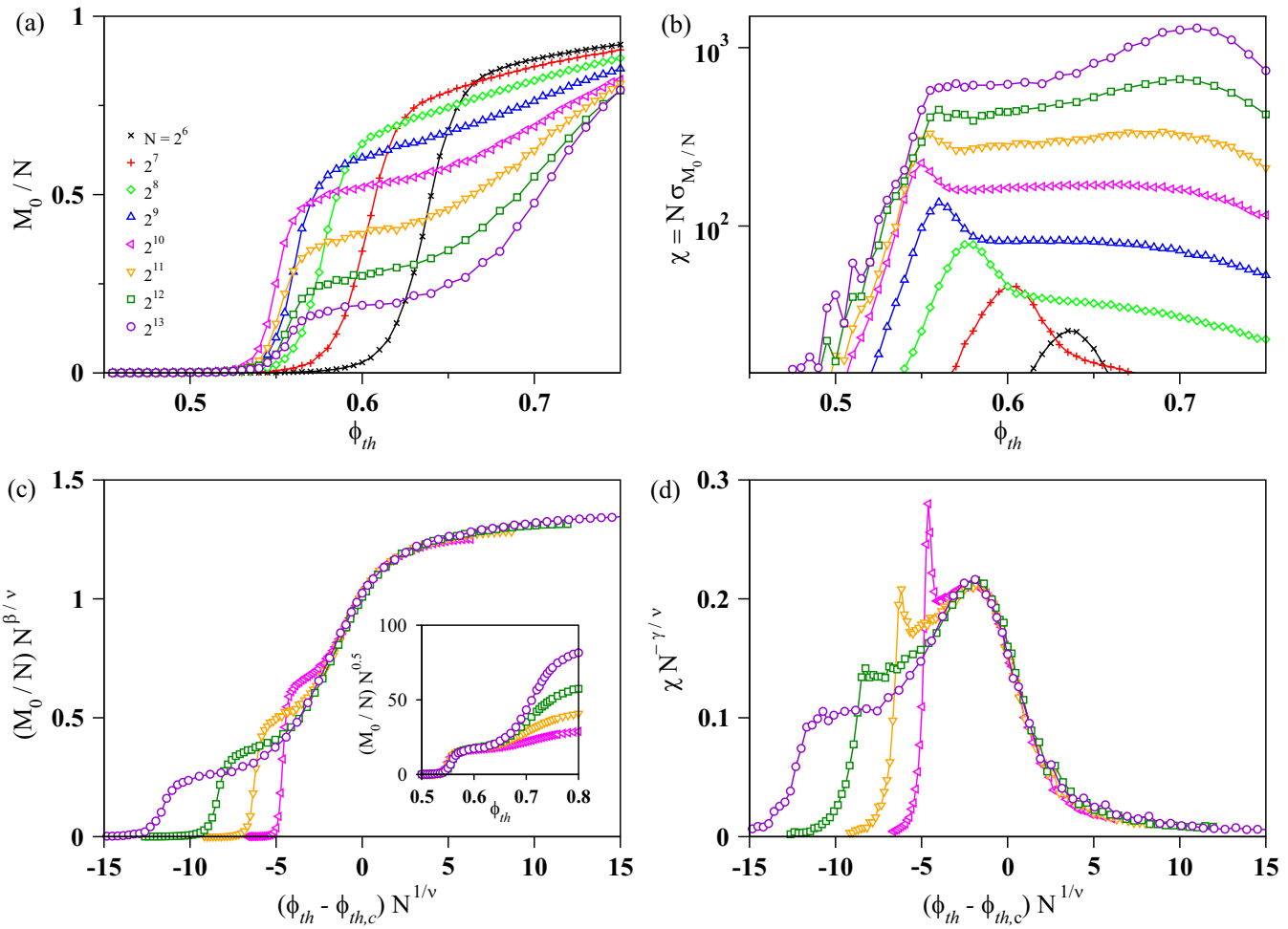

FIG. 3. (a) The dependence of the size of the largest cluster of nonaligners M_0 on the threshold $\phi_{\rm th}$ at noise $\eta = 0.2$ and density $\rho = 1.6$. The different symbols correspond to different system sizes N, as indicated in the legend. The curves reveal a system size dependent crossover occurring at $N \sim 2^{10}$. For larger systems M_0 has an initial steep rise and then a gradual increase. (b) A susceptibility function χ corresponding to M_0 is shown, where $\chi = N\sqrt{\langle (M_0/N)^2\rangle - \langle (M_0/N)\rangle^2}$. From around the crossover system size a second peak in χ starts becoming the dominant maximum. The first peak corresponds to $\phi_{\rm th} = \phi^*$, and the second peak corresponds to the second increase of M_0 at $\phi_{\rm th} = \phi_{\rm th,c}$. (c) Curves from (a) with system sizes from $N \sim 2^{10}$ and above are rescaled. By plotting $(M_0/N)N^{\beta/\nu}$ versus $(\phi_{\rm th} - \phi_{\rm th,c})N^{1/\nu}$ the validity of Eq. (7) is illustrated. Here, $\phi_{\rm th,c} = 0.74$. The inset shows $(M_0/N)N^{0.5}$ versus $\phi_{\rm th}$. The collapse shows that the initial rise of M_0 at $\phi_{\rm th} = \phi^*$ occurs according to $M_0 \sim N^{0.5}$. (d) The collapse of the second peak of susceptibility [from (b)] is obtained following a procedure similar to that in (c). This demonstrates the scaling ansatz in Eq. (8).

dependence on N is qualitatively similar in both cases. While for $v_0 = 0$ the ejection of aligners from a cluster of nonaligners occurs due to random switching events, for $v_0 > 0$ there is an additional diffusion of the nonaligner particles before the switchings happen. In Sec. III D we show the dependence of M_0 on v_0.

The abrupt increase in M_0 as $\phi_{\rm th}$ increases in the low noise regime coincides with a decrease in the size of the largest cluster of aligners M_1. This is visible in Fig. 2(d), where M_1 is plotted as a function of $\phi_{\rm th}$ for different N at $\eta = 0.2$. By tuning the exponent in the relation $M_1 \sim N^{\zeta_1}$ we obtain the best collapse for different N with $\zeta_1 = 0.78$.

B. High density regime

In the high density and low noise regime, we observe the largest cluster of nonaligners grows with $\phi_{\rm th}$, whose size is of the order of N when $\phi_{\rm th}$ is unity. An incipient cluster in this regime is shown in Fig. 1 (top row, third from the left). In addition, we find the behavior of the system to be strongly dependent on N. In Fig. 3(a) we plot the fraction M_0/N for different system sizes. From the different curves we observe that the generic dependence of M_0/N on $\phi_{\rm th}$ is different for smaller and larger values of N, with a crossover occurring at $N \sim 2^{10}$. For the smaller systems the growth in the largest cluster primarily occurs when $\phi_{\rm th}$ is between 0.6 and 0.7. For the larger systems there is an initial rapid increase in M_0 that is similar to that observed at low densities that is followed by gradual further growth.

Considering the growth of the larger cluster of nonaligners to be a percolation phenomenon that occurs with respect to the tuning of $\phi_{\rm th}$, we calculate the susceptibility corresponding to the order parameter M_0/N, given by $\chi = N\sigma$, with $\sigma^2 = \langle (M_0/N)^2\rangle - \langle (M_0/N)\rangle^2$ [46], where the angular brackets

denote averaging in the steady state. The plot of χ as a function of $\phi_{\rm th}$ in Fig. 3(b) demonstrates a crossover in the finite-size effect. For $N < 2^{10}$ there is only a single maximum that shifts to the left of the $\phi_{\rm th}$ axis on increasing N. With $N \geqslant 2^{10}$ we find the emergence of a second peak in χ which is the dominant maximum as N increases further. Ideally, for a given N, the position of the (second) maximum of χ is expected to provide the critical thresholds (pseudocritical point) $\phi_{\rm th,c}(N)$. Observing that accurately locating the second maximum can be difficult for the smaller system sizes, we circumvent the problem in the following way. For the finite-size effects in percolation we assume the relations

$$M_0/N = N^{-\beta/\nu}\mathcal{F}\big[(\phi_{\rm th} - \phi_{\rm th,c})N^{1/\nu}\big], \tag{7}$$

$$\chi = N^{\gamma/\nu}\mathcal{G}\big[(\phi_{\rm th} - \phi_{\rm th,c})N^{1/\nu}\big], \tag{8}$$

where $\phi_{\rm th,c}$ is the critical threshold in the infinite-size limit ($N \to \infty$) and ν, β, and γ are the critical exponents characterizing a second order percolation transition. Using the above relations and the fact that $\chi = N\sigma$, we get a hyperscaling relation,

$$\gamma/\nu = 1 - \beta/\nu. \tag{9}$$

At different values of $\phi_{\rm th}$ we fit power laws to the data corresponding to M_0/N versus N. This gives us a set of trial values for the exponent β/ν. Similarly, we obtain a set of trial values of γ/ν from χ versus N at different $\phi_{\rm th}$. Then we obtain the critical point $\phi_{\rm th,c}$ by locating the $\phi_{\rm th}$ at which β/ν and γ/ν satisfy Eq. (9). This method yields $\beta/\nu = 0.035(9)$, $\gamma/\nu = 0.965(4)$, and $\phi_{\rm th,c} = 0.740(5)$. The error estimates in the exponents correspond to power-law fits at ± 0.005 from $\phi_{\rm th,c}$. (In the Appendix we provide expressions for M_0 and $\phi_{\rm th,c}$ from a reaction-limited description.)

To determine ν, we first scale the y axis of Fig. 3(a) by multiplying by $N^{\beta/\nu}$. Then upon fixing a value of $(M_0/N)N^{\beta/\nu}$ around 1.0 we obtain the corresponding values of $\phi_{\rm th}$ for different N. We estimate the value of $1/\nu$ from the slope of the line fitted with $\log|\phi_{\rm th}(N) - \phi_{\rm th,c}|$ versus $\log N$. Repeating the process for different values of $(M_0/N)N^{\beta/\nu}$, we get $\nu = 2.16(3)$. Using the above values for the scaling exponents and $\phi_{\rm th,c}$, we obtain data collapses for M_0/N and χ, as shown in Figs. 3(c) and 3(d), respectively. The collapse of the curves for different N when $\phi_{\rm th}$ is close to $\phi_{\rm th,c}$ shows that the scaling forms in Eqs. (7) and (8) hold true.

Similar to the case of low density, there is an initial rapid increase in M_0 at $\phi_{\rm th} = \phi^*$. This is characterized by solely scaling the M_0/N axis and collapsing the curves for different N, as shown in the inset of Fig. 3(c). The scaling shows that as $\phi_{\rm th}$ crosses ϕ^*, M_0 abruptly increases from $O(1)$ to $O(\sqrt{N})$. The latter increase in M_0 also coincides with a fall in M_1 (not shown). For $\phi_{\rm th} < \phi^*$ we find $M_1 \sim N^{\zeta_2}$ with $\zeta_2 = 0.80$, which is quite close to ζ_1.

Additionally, we also studied the cluster size distribution of the nonaligners. We obtained the statistics by observing the systems at $\phi_{\rm th} = \phi_{\rm th,c}$. The normalized distributions $n(m_0)$ for the cluster sizes m_0 of nonaligners are plotted in Fig. 4(a) for different N. We assume power-law distributed cluster sizes and finite-size effects are present, such that $n(m_0) \sim m_0^{-\tau} f(m_0/M_0)$, where τ is the Fisher exponent. With the system being at $\phi_{\rm th,c}$ we expect $M_0 \sim N^{\epsilon_1}$, with $\epsilon_1 = 1 - \beta/\nu$, and therefore, the above power law can be recast into the following form:

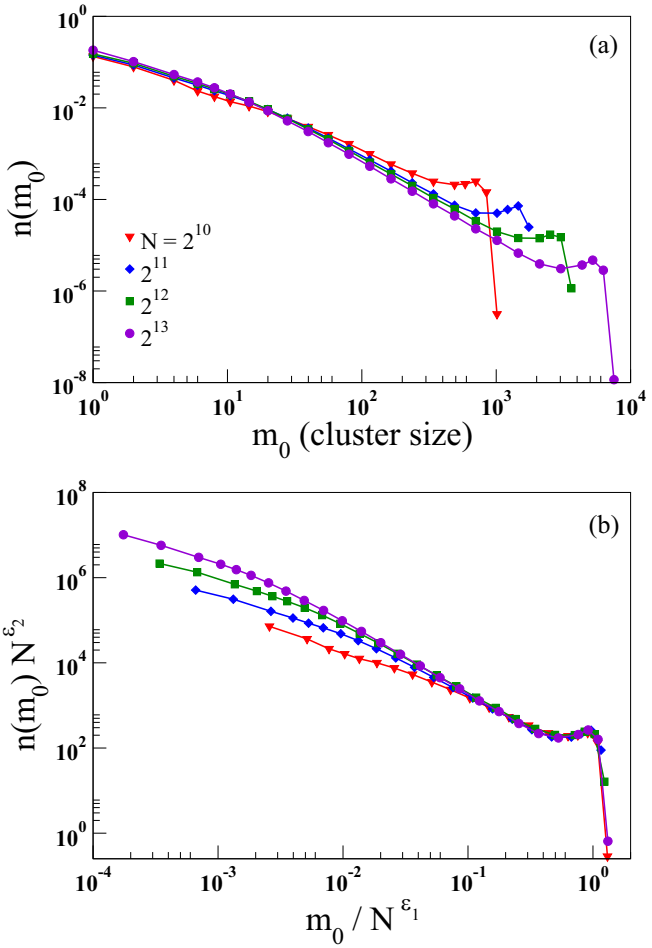

FIG. 4. (a) Normalized distributions of cluster sizes of nonaligners for different system sizes, indicated in the legend. The distributions have been obtained at $\eta = 0.2$, $\rho = 1.6$, and $\phi_{\rm th} = 0.74 = \phi_{\rm th,c}$. (b) A collapse of the distributions from (a), obtained by plotting $n(m_0)N^{\epsilon 2}$ versus m_0/N^{ϵ_1} and tuning ϵ_1 and ϵ_2. In (b) $\epsilon_1 = 0.96(2)$ and $\epsilon_2 = 1.98(1)$. The collapse indicates a power law $n(m_0) \sim {m_0}^{-\tau}$ in the large N limit with $\tau = \epsilon_2/\epsilon_1 = 2.06(3)$.

$$n(m_0) = N^{-\epsilon_2}D(m_0/N^{\epsilon_1}), \tag{10}$$

where the scaling function $D(x) \sim x^{-\tau}$ for $x \to 0$ and $D(x)$ decreases faster than a power law for $x \gg 1$. This implies $\tau = \epsilon_2/\epsilon_1$. In Fig. 4(b) we plotted $n(m_0)N^{\epsilon_2}$ versus m_0/N^{ϵ_1} and tuned the values of ϵ_1 and ϵ_2 to get a collapse of the distribution for different N. The latter allows us to validate Eq. (10). We get the best collapse for $\epsilon_1 = 0.96(2)$ and $\epsilon_2 = 1.98(1)$, which implies $\tau = 2.06(3)$.

C. Generic dependence on density

After observing that switching of particle states in ordered flocks produces two distinct type of mixed phases, nonpercolating and percolating, depending on the density ρ, we investigate how the relevant quantities continuously vary as a function of ρ. In Fig. 5 we show the variation of M_0 and M_1 at

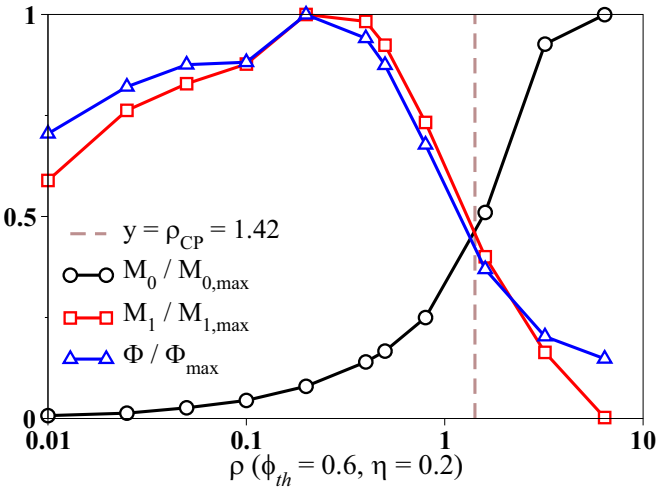

FIG. 5. The following quantities of interest are plotted as a function of density ρ at noise $\eta = 0.2$ and threshold $\phi_{\text{th}} = 0.6$: $M_0/M_{0,\text{max}}$, the size of the largest cluster of nonaligners normalized by its maximum value within the range of investigation; $M_1/M_{1,\text{max}}$, the normalized size of the largest cluster of aligners; and Φ/Φ_{max}, the normalized polarization of the system. The dashed vertical line indicates the density that corresponds to the critical filling factor for continuum percolation, $\rho_{\text{CP}} = 1.42$.

low noise ($\eta = 0.2$) and a substantial presence of switching activity ($\phi_{\text{th}} = 0.6$). In addition to the sizes of the largest clusters we also show the polarization Φ [2,9], which is a measure of the degree of global order in the system and is defined as $\Phi = \langle |(1/N) \sum_{i=1,N} \mathbf{n}_i^t| \rangle$.

We compare M_0, M_1, and Φ scaled by their respective maximum values with ρ being in the range 0.01 to 10.0. It is known that in a pure SPP system for a fixed η, long-range order vanishes when density is lowered [47]. This phenomenon partially underlies the dynamics observed in our case where switching is allowed. The relatively low degree of order as reflected in the values of $M_1/M_{1,\text{max}}$ and Φ/Φ_{max} at very low densities is the result of a lack of order in the pure system. The maximum in the values of M_1 and Φ occurs at around $\rho \gtrsim 0.1$. In this regime, the absence of switching implies that the system has a high degree of order and a macroscopically large cluster of aligners always exists in the steady state. When switching is present, we observe the nonpercolating mixed phase where $M_0 \sim \log N$. A further increase in the density would result in the enhancement of order and aligner cluster size in the pure system. However, for the mixed phase the aligner cluster size and order decrease with a further increase in density. The cluster size for nonaligners increases monotonically. The possibility of the formation of a giant cluster of nonaligners may be considered to be similar to the situation of continuum percolation (CP) of overlapping disks with radii $R = r_0/2$. Noting that the filling fraction is defined as $\pi R^2 \rho$ and that the estimate for the critical value is around 1.12 [48], the corresponding critical density is $\rho_{\text{CP}} = 1.42$. This density, therefore, would signify the border between nonpercolating and percolating mixed phases. The latter is evident in the case of $\rho = 1.6 > \rho_{\text{CP}}$.

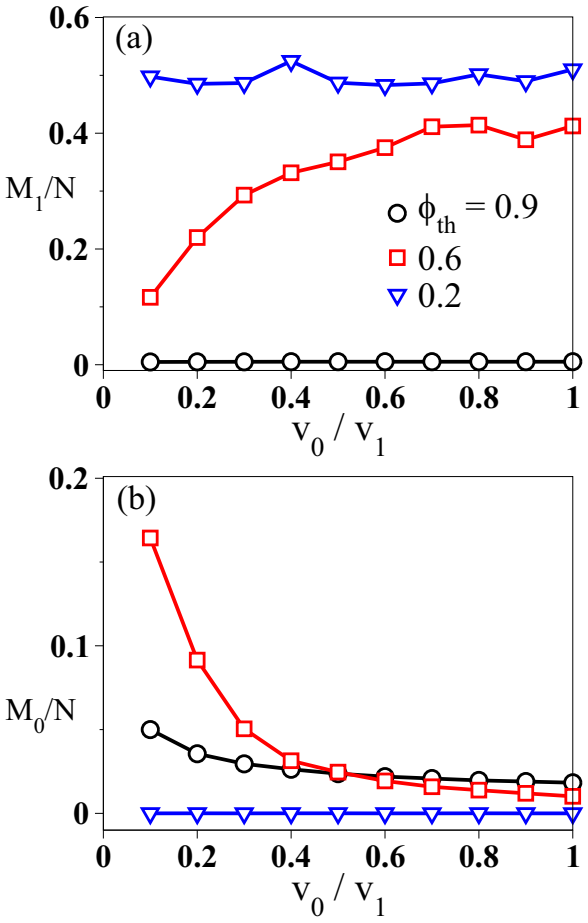

FIG. 6. (a) Dependence of the size of the largest cluster of aligners M_1 on nonaligner speed v_0 for three different thresholds ϕ_{th}. The aligner speed $v_1 = 0.05$, noise $\eta = 0.2$, number of particles $N = 1024$, and density $\rho = 0.5$. (b) Dependence of the size of the largest cluster of nonaligners M_0.

D. Dependence on speed differences

Last, we study how the difference between the speeds of the aligners and nonaligners governs the evolution of the system. We fix the aligner speeds to $v_1 = 0.05$ and vary the speed of the nonaligners, v_0. We plot M_1 and M_0 as functions of v_0 for three different values of ϕ_{th} in Fig. 6. It is apparent that the mixed phase ($\phi_{\text{th}} = 0.6$) where macroscopically large aligner and nonaligner clusters coexist is delicately dependent on the value of v_0. As v_0 approaches v_1, M_0 is found to decrease, and M_1 is found to increase. The diffusion of nonaligners occurs with a diffusion constant that is proportional to v_0^2 [44,49]. Therefore, the rate of ejection of aligners from the boundary of a cluster of nonaligners also increases as the nonaligner speed is increased. In addition, as the relative difference in speeds vanishes, the nonaligners formed after a collision effectively fail to segregate and, eventually, to proliferate. As a result of the above, the effect of a finite ϕ_{th} diminishes, and large clusters of nonaligners are rarely observed. These results show that the formation of mixed phases that is controlled by ϕ_{th} is also dependent on the difference in speeds. We have shown the dependence on v_0 in the nonpercolating regime, but the indications are similar for the percolating case as well.

IV. CONCLUSIONS

We studied a system in which self-propelled particles were allowed to switch states between fast aligners and slow nonaligners based on the degree of alignment in their neighborhood. In the steady state, the system segregated into separate clusters of aligners and nonaligners. In the mixed phase, the largest cluster of aligners was found to vary algebraically with the system size. However, depending on the density of the system, the aggregation of the nonaligners appeared to be very different. For low densities, the largest cluster of nonaligners reached a maximum size for an optimal noise and an optimal threshold. For high densities, after an initial abrupt increase, a giant percolating cluster could emerge with the increase in the threshold. Also, the behavior for small system sizes appeared to be very different. The boundary between the density regimes roughly coincided with the density corresponding to the critical filling factor for a continuum percolation transition. Irrespective of the density, the separation of speeds seemed to be a necessary condition for the model to display the segregation of nonaligners. When the speeds become comparable, large clusters of nonaligners are predominantly absent. Although the appearance of the giant cluster conforms to a set of finite-size scaling hypotheses, the transition could be nonuniversal [50] with dependence on the noise amplitude and density, through the functions $\mathcal{F}$ and $\mathcal{G}$ in Eqs. (7) and (8).

The percolation of clusters was recently studied [51] in the classical Vicsek model. Unlike our model, the SPPs in the Vicsek model always remain aligners (without switching), and attraction-repulsion forces are absent. The authors investigated the global connectivity of clusters with an increase in the global density ρ along both the longitudinal and transverse directions with respect to the direction of global order. They estimated a critical density $\rho_c = 1.96\,(> \rho_{\mathrm{CP}})$. Similar to the current model, if we denote the size of the largest cluster (of aligners) in the Vicsek model as M_1, then close to ρ_c, the dependence on N may be characterized by using $M_1 \sim N^{\zeta}$. Using the reported [51] values of the different critical exponents, ζ is found be in the range 0.95–1.00. In our model, for the density regimes investigated and when the clusters of aligners are macroscopically large ($\phi_{\mathrm{th}} < \phi^*$), we find ζ to be in the range 0.78–0.80. Taken together, we believe that our model was investigated at densities which are still lower than the critical density that would be needed for the percolation of clusters of aligners if switching is absent. Also note that in our model, clusters of nonaligners are formed mainly due to the collisions between clusters and the speed difference between aligners and nonaligners.

Recent advances in living active matter have found that modifications in individual behavior through the sensing of local densities lead to the formation of regions of orientational disorder and aggregations [52–55]. Similar observations have been made in experiments with active colloidal systems employing different methods to program the particle motion, like optical feedback loops and field modulations [55–57]. Therefore, the observed macroscopic behavior in our model could be relevant, for example, to active colloids with setups allowing the particles to sense and respond to the average orientation of neighbors [58], to the design and control of robot swarms [6,59], and, in general, to systems exhibiting both polar order and MIPS-related behavior [34,60,61]. Also, owing to the additional state variable in our model, the latter can be contrasted with the study of clustering and percolation in the classical Vicsek model [51], and similarities with models for information spreading in motile collectives can be further explored [36,37].

Also, there appears to be scope for additional complexity in the current model. We have assumed that switching behavior is symmetric in terms of having a single threshold for both aligners and nonaligners. In a more general scheme, there can be two different thresholds for particles of either type. Currently, the additive noise causes the moving clusters to collide, which generates the nonaligners. It would be interesting to test the model at zero noise [62] but with other forms of disorder like boundaries, obstacles [8], and quenched nonaligners [10]. The phase separation between aligners and nonaligners could also be studied in systems without self-propulsion, for example, in Brownian walkers with a velocity alignment interaction [63] and in the Vicsek model on the lattice [64].

ACKNOWLEDGMENTS

K.B. and A.C. acknowledge helpful discussions with S. N. Menon, S. Vijayakumar, and S. Kundu.

APPENDIX: MEAN FIELD DESCRIPTION

Here, we provide a reaction-limited description of the system in the high density regime based on our simulations and neglecting the spatial correlations. We consider the system to consist of the following types of particles: particles that are part of the giant cluster of nonaligners (M_0), aligners (N_1), and nonaligners that are not part of the giant cluster (N_0'), such that

$$M_0 + N_0' + N_1 = N. \tag{A1}$$

As seen with regard to Fig. 3, as ϕ_{th} crosses ϕ^*, M_0 becomes $O(\sqrt{N})$. On further increasing ϕ_{th}, when the latter reaches $\phi_{\mathrm{th,c}}$, the incipient giant cluster is observed. We model the growth of this cluster using the following equation:

$$\frac{dM_0}{dt} = (\phi_{\mathrm{th}} - \phi^*)AM_0N_1 - (1 - \phi_{\mathrm{th}})BM_0. \tag{A2}$$

The first term to the right accounts for the collision between the aligner particles and the giant cluster of nonaligners by which particles are added to the perimeter of the latter. Given that a percolating cluster is growing and is far from being circular in shape, the perimeter is assumed to vary as M_0. A typical snapshot of such a cluster is shown in Fig. 1 (top row, third from the left). In general, for a percolating cluster the relation between the perimeter (or hull) and the mass is given by $H_0 \sim {M_0}^x$, with $x = d_h/d_f$. Here, d_f and d_h are the fractal and hull dimensions, respectively, and can be computed using the relations $d_f = d - \beta/\nu_L$ and $d_h = 1 + 1/\nu_L$ [65,66]. In the current context, the exponents from our numerical calculations in Sec. III B would indicate $x \approx 1$. The exponent $\nu_L = \nu/d$, where the dimensionality of space $d = 2$. For classical percolation in $d = 2$, $d_f = 91/48$, and $d_h = 7/4$, which gives $x \simeq 0.92$ [66]. On the other hand, clusters of

aligners are mostly small in size in this regime; therefore, the dependence is taken to be proportional to the total number of aligners N_1. The colliding aligners are expected to have their local order parameter distributed around ϕ^*. Keeping other factors unchanged, as $\phi_{\rm th}$ approaches ϕ^* from below and eventually crosses ϕ^*, more and more aligners are expected to switch their states. We approximate this dependence on $\phi_{\rm th}$ as $\phi_{\rm th} - \phi^*$. The coefficient A contains factors in the collision rate, including the speed of the group of aligners [44,49], and is independent of $\phi_{\rm th}$. The second term accounts for the loss of particles by which particles near the perimeter of the giant cluster switch to aligning states and detach from the latter. While within the bulk the local order parameter would typically be around $r_e/(2r_0)$ [see discussion on Fig. 2(b)], for the nonaligners at the boundary we expect larger fluctuations and hence a flatter distribution extending up to unity. We assume that the rate of switching is proportional to $1 - \phi_{\rm th}$. The coefficient B takes into account other factors independent of $\phi_{\rm th}$.

We observe in our simulations that apart from the ones in the giant cluster, the nonaligners are formed in the process of collision between small clusters of nonaligners. The resulting clusters of nonaligners are also small and are not stable. We model this process using the following equation:

$$\frac{dN_0'}{dt} = (\phi_{\rm th} - \phi^*)kAN_1{}^2 - (1 - \phi_{\rm th})BN_0'. \tag{A3}$$

The first term accounts for the formation of the small clusters of nonaligners. We assume that the coefficient in the collision rate accounting for factors independent of time and $\phi_{\rm th}$ is different by only a multiplicative constant from the coefficient in Eq. (A2). The second term is similar to the loss term in dM_0/dt.

We are interested in the steady state dependence of M_0 on $\phi_{\rm th}$. Therefore, we set the right hand side of Eq. (A2) to zero. Assuming a nonzero finite solution for M_0, we get the following steady solution for N_1:

$$N_1^s = bf(\phi_{\rm th}), \tag{A4}$$

where $f(\phi_{\rm th}) = (1 - \phi_{\rm th})/(\phi_{\rm th} - \phi^*)$ and $b = B/A$. Similarly, by equating the right hand side of Eq. (A3) to zero, we get $N_0'^s = kN_1^s$. Next, the steady state solution for M_0 is found by using N_1^s and $N_0'^s$ in Eq. (A1):

$$M_0^s = N - b(1 + k)f(\phi_{\rm th}). \tag{A5}$$

In Fig. 7 we compare the steady state solutions for N_1, N_0', and M_0 with the numerical results. As mentioned above, the derived expression appears to be valid for $\phi_{\rm th} > \phi_{\rm th,c}$ when the incipient giant cluster is already present. Below $\phi_{\rm th,c}$, clusters of nonaligners keep continually forming and fragmenting, clusters of aligners are relatively larger in size, and spatial correlations cannot be neglected in the description of the dynamics.

Considering that the collision coefficient A is inversely proportional to the area L^2 [44,49], we can also rewrite

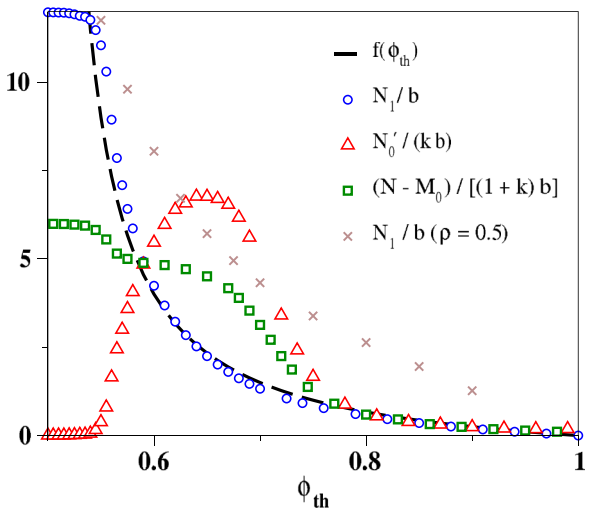

FIG. 7. Results from the simulation in the high density regime ($\rho = 1.6$, $\eta = 0.2$, and $N = 2^{13}$) are compared with the steady state solutions from the model. The dashed line denotes the function $f(\phi_{\rm th}) = (1 - \phi_{\rm th})/(\phi_{\rm th} - \phi^*)$. The circles show the dependence on $\phi_{\rm th}$ for the number of aligners N_1 scaled by a constant b. Choosing $b/N \approx 1/12$ shows the validity of Eq. (A4). Similarly, the triangles and squares show the ranges of validity for the relation $N_0' = kN_1$ and Eq. (A5), respectively, where $k = 1$. The plot of N_1/b in the low density regime is shown using the crosses. Here, we take $\phi^* = 0.5$, which provides the best fit instead of $\phi^* = 0.47$, which is obtained from Eq. (6).

Eq. (A5) as

$$M_0^s = N[1 - (c/\rho)f(\phi_{\rm th})], \tag{A6}$$

where $c/\rho = b(1 + k)/N$. The above expressions for M_0^s imply that when N increases at a fixed density or when ρ increases, the transition to a global connectivity becomes faster. This expression, however, is not valid in the limit $\rho \to 0$. For the latter limit in Eq. (A2), the second term would be the dominant term for all values of $\phi_{\rm th}$, and M_0 would be zero in the steady state. Alternately, the dynamics at low density cannot be described by Eqs. (A2) and (A3), and as a result, Eq. (A4) does not hold. The deviation of N_1^s/b at low density from the function $f(\phi_{\rm th})$ is shown in Fig. 7.

We obtain an estimate of $\phi_{\rm th,c}$ by assuming that once the critical threshold is exceeded, the number of nonaligners inside the largest cluster becomes greater than the number of nonaligners present outside: $M_0^s > N_0'^s$. Here, using the expressions M_0^s and $N_0'^s$, we get a lower bound on $\phi_{\rm th}$,

$$\phi_{\rm th,c} = \phi^* + \frac{3c}{3c + 2\rho}(1 - \phi^*), \tag{A7}$$

where we have set $k = 1$ as shown in Fig. 7. Therefore, in this reaction dominated description, the limits $N \to \infty$ at a fixed density or $\rho \to \infty$ imply that $\phi_{\rm th,c} \to \phi^*$ from above. Finally, given that the function $f(\phi_{\rm th})$ is analytic in the range $\phi^* < \phi_{\rm th} \leqslant 1$, we can express as a first order approximation $M_0^s(\phi_{\rm th}) - M_0^s(\phi_{\rm th,c}) \sim (\phi_{\rm th} - \phi_{\rm th,c})$ for $\phi_{\rm th} \gtrsim \phi_{\rm th,c}$, giving $\beta(\text{mean field}) = 1$.

[1] A. Huth and C. Wissel, Ecol. Modell. **75**, 135 (1994).
[2] A. Cavagna, A. Cimarelli, I. Giardina, G. Parisi, R. Santagati, F. Stefanini, and M. Viale, Proc. Natl. Acad. Sci. USA **107**, 11865 (2010).
[3] A. Czirók, E. Ben-Jacob, I. Cohen, and T. Vicsek, Phys. Rev. E **54**, 1791 (1996).
[4] J. L. Silverberg, M. Bierbaum, J. P. Sethna, and I. Cohen, Phys. Rev. Lett. **110**, 228701 (2013).
[5] J. Elgeti, R. G. Winkler, and G. Gompper, Rep. Prog. Phys. **78**, 056601 (2015).
[6] M. Rubenstein, A. Cornejo, and R. Nagpal, Science **345**, 795 (2014).
[7] T. Vicsek, A. Czirók, E. Ben-Jacob, I. Cohen, and O. Shochet, Phys. Rev. Lett. **75**, 1226 (1995).
[8] O. Chepizhko, E. G. Altmann, and F. Peruani, Phys. Rev. Lett. **110**, 238101 (2013).
[9] K. Copenhagen, D. A. Quint, and A. Gopinathan, Sci. Rep. **6**, 31808 (2016).
[10] D. Yllanes, M. Leoni, and M. Marchetti, New J. Phys. **19**, 103026 (2017).
[11] O. Chepizhko and F. Peruani, Phys. Rev. Lett. **111**, 160604 (2013).
[12] L. Conradt and T. J. Roper, Trends Ecol. Evol. **20**, 449 (2005).
[13] O. Petit and R. Bon, Behav. Processes **84**, 635 (2010).
[14] K. Bhattacharya and T. Vicsek, J. R. Soc. Interface **11**, 20140674 (2014).
[15] J. Buhl, D. J. Sumpter, I. D. Couzin, J. J. Hale, E. Despland, E. R. Miller, and S. J. Simpson, Science **312**, 1402 (2006).
[16] I. Daruka, Proc. R. Soc. B **276**, 911 (2009).
[17] N. Miller and R. Gerlai, PLoS One **7**, e48865 (2012).
[18] F. Ginelli, F. Peruani, M.-H. Pillot, H. Chaté, G. Theraulaz, and R. Bon, Proc. Natl. Acad. Sci. USA **112**, 12729 (2015).
[19] W. Li and X. Wang, Phys. Rev. E **75**, 021917 (2007).
[20] F. D. C. Farrell, M. C. Marchetti, D. Marenduzzo, and J. Tailleur, Phys. Rev. Lett. **108**, 248101 (2012).
[21] K. Bhattacharya and T. Vicsek, New J. Phys. **12**, 093019 (2010).
[22] Y. Katz, K. Tunstrøm, C. C. Ioannou, C. Huepe, and I. D. Couzin, Proc. Natl. Acad. Sci. USA **108**, 18720 (2011).
[23] K. Tunstrøm, Y. Katz, C. C. Ioannou, C. Huepe, M. J. Lutz, and I. D. Couzin, PLoS Comput. Biol. **9**, e1002915 (2013).
[24] L. H. Cisneros, J. O. Kessler, S. Ganguly, and R. E. Goldstein, Phys. Rev. E **83**, 061907 (2011).
[25] S. Mishra, K. Tunstrøm, I. D. Couzin, and C. Huepe, Phys. Rev. E **86**, 011901 (2012).
[26] J. P. Singh and S. Mishra, Phys. A (Amsterdam, Neth.) **544**, 123530 (2020).
[27] M. E. Cates and J. Tailleur, Annu. Rev. Condens. Matter Phys. **6**, 219 (2015).
[28] J. Tailleur and M. E. Cates, Phys. Rev. Lett. **100**, 218103 (2008).
[29] Y. Fily and M. C. Marchetti, Phys. Rev. Lett. **108**, 235702 (2012).
[30] D. Martin, J. O'Byrne, M. E. Cates, É. Fodor, C. Nardini, J. Tailleur, and F. van Wijland, Phys. Rev. E **103**, 032607 (2021).
[31] S. R. McCandlish, A. Baskaran, and M. F. Hagan, Soft Matter **8**, 2527 (2012).
[32] J. Barré, R. Chétrite, M. Muratori, and F. Peruani, J. Stat. Phys. **158**, 589 (2015).
[33] E. Sese-Sansa, I. Pagonabarraga, and D. Levis, Europhys. Lett. **124**, 30004 (2018).
[34] M. N. van Der Linden, L. C. Alexander, D. G. A. L. Aarts, and O. Dauchot, Phys. Rev. Lett. **123**, 098001 (2019).
[35] G. Grégoire and H. Chaté, Phys. Rev. Lett. **92**, 025702 (2004).
[36] M. Paoluzzi, M. Leoni, and M. C. Marchetti, Phys. Rev. E **98**, 052603 (2018).
[37] M. Paoluzzi, M. Leoni, and M. C. Marchetti, Soft Matter **16**, 6317 (2020).
[38] I. D. Couzin, J. Krause, R. James, G. D. Ruxton, and N. R. Franks, J. Theor. Biol. **218**, 1 (2002).
[39] G. Grégoire, H. Chaté, and Y. Tu, Phys. D (Amsterdam, Neth.) **181**, 157 (2003).
[40] See Supplemental Material at http://link.aps.org/supplemental/10.1103/PhysRevE.105.044124 for numerical simulations, relevant length scales and timescales, and movies of the dynamics, which includes Refs. [67,68].
[41] A. P. Solon, J.-B. Caussin, D. Bartolo, H. Chaté, and J. Tailleur, Phys. Rev. E **92**, 062111 (2015).
[42] H. Chaté, Annu. Rev. Cond. Matt. Phys. **11**, 189 (2020).
[43] F. Ginelli, Eur. Phys. J.: Spec. Top. **225**, 2099 (2016).
[44] F. Peruani, L. Schimansky-Geier, and M. Baer, Eur. Phys. J.: Spec. Top. **191**, 173 (2010).
[45] V. Dossetti, F. J. Sevilla, and V. M. Kenkre, Phys. Rev. E **79**, 051115 (2009).
[46] F. Radicchi and S. Fortunato, Phys. Rev. Lett. **103**, 168701 (2009).
[47] A. Czirók and T. Vicsek, Phys. A (Amsterdam, Neth.) **281**, 17 (2000).
[48] S. Mertens and C. Moore, Phys. Rev. E **86**, 061109 (2012).
[49] F. Peruani and M. Baer, New J. Phys. **15**, 065009 (2013).
[50] Y. Liu and R. B. Pandey, Phys. Rev. B **55**, 8257 (1997).
[51] N. Kyriakopoulos, H. Chaté, and F. Ginelli, Phys. Rev. E **100**, 022606 (2019).
[52] H. Ling, G. E. Mclvor, J. Westley, K. van der Vaart, R. T. Vaughan, A. Thornton, and N. T. Ouellette, Nat. Commun. **10**, 1 (2019).
[53] S. E. Leggett, Z. J. Neronha, D. Bhaskar, J. Y. Sim, T. M. Perdikari, and I. Y. Wong, Proc. Natl. Acad. Sci. USA **116**, 17298 (2019).
[54] P. P. Klamser, L. Gómez-Nava, T. Landgraf, J. W. Jolles, D. Bierbach, and P. Romanczuk, Front. Phys. **9**, 516 (2021).
[55] T. Bäuerle, A. Fischer, T. Speck, and C. Bechinger, Nat. Commun. **9**, 3232 (2018).
[56] F. A. Lavergne, H. Wendehenne, T. Bäuerle, and C. Bechinger, Science **364**, 70 (2019).
[57] R. Soma, B. Nakayama, M. Kuwahara, E. Yamamoto, and T. Saiki, Appl. Phys. Lett. **117**, 221601 (2020).
[58] T. Bäuerle, R. C. Löffler, and C. Bechinger, Nat. Commun. **11**, 1 (2020).
[59] J. Werfel, K. Petersen, and R. Nagpal, Science **343**, 754 (2014).
[60] E. Crosato, M. Prokopenko, and R. E. Spinney, Phys. Rev. E **100**, 042613 (2019).
[61] E. Sesé-Sansa, D. Levis, and I. Pagonabarraga, Phys. Rev. E **104**, 054611 (2021).
[62] A. Chakraborty and K. Bhattacharya, Europhys. Lett. **116**, 48001 (2016).

[63] V. Dossetti and F. J. Sevilla, Phys. Rev. Lett. **115**, 058301 (2015).
[64] B. Bhattacherjee, K. Bhattacharya, and S. S. Manna, Front. Phys. **1**, 35 (2014).
[65] H. Saleur and B. Duplantier, Phys. Rev. Lett. **58**, 2325 (1987).
[66] D. Stauffer and A. Aharony, *Introduction to Percolation Theory*, revised 2nd ed. (Taylor and Francis, Philadelphia, 2003).
[67] M. Allen and D. Tildesley, *Computer Simulation of Liquids* (Clarendon, Oxford, 1987).
[68] J. Hoshen and R. Kopelman, Phys. Rev. B **14**, 3438 (1976).